Journal of Engineering Science and Technology
Vol. 16, No. 3 (2021) 2544 - 2561

AN EXTENDED VALIDATION OF FREE CFD APPLICATION TO SHIP RESISTANCE PREDICTION FOR USING IN PRELIMINARY DESIGN STAGE

S. BASO*, A. ARDIANTI, ROSMANI, A. D. E. ANGGRIANI

Naval Architecture Department, Faculty of Engineering, Hasanuddin University
Jalan Perintis Kemerdekaan Km.10, 90245, Makassar, Indonesia
*Corresponding Author: s.baso@eng.unhas.ac.id

Abstract

Nowadays, Computational Fluid Dynamics (CFD) has gained high popularity for ship resistance prediction because of its high efficiency and economics. Correspondingly, over the years, the accuracy and ability of CFD have been widely strived to be improved. Therefore, these research objectives are to apply the free CFD application (Autodesk CFD) for predicting pressure distribution, fluid velocity around a ship, and resistance of a ship hull from Fr 0.019 to 0.213 and then to investigate a discrepancy between Autodesk CFD results and experimental results. The Autodesk CFD governs Navier-Stokes's equations which are solved by using the Finite Element Method (FEM). Then, the experimental work was carried out in the same condition with the computation wherein the resistance test was conducted into four Froude numbers Fr 0.058, 0.116, 0.174, and 0.213. Also, the experimental pressure distribution along the model hull was measured by using the piezoelectric device. The comparisons of the peak pressure coefficient *Cp* on the bow surface BB (model with a bulbous bow) and WBB (model without bulbous bow) between experimental results and the computational result are given different magnitudes 4.88% and 5.23% respectively. Also, the computational result of the water-resistance coefficient *Ct* in the increasing of the Fr has a similar tendency with the experimental result for both model BB and WBB. The different value of the *Ct* between computation and experiment for model BB is averaged 3.59% and then for model WBB, the different value has obtained the average of 4.86%. The overall computational results confirm good agreement with the experimental results. Then, by the differences, the free Autodesk CFD application could be tolerable to be used practically in the preliminary ship design stage.

Keywords: Autodesk CFD, Pressure distribution, Ship design, Ship resistance, Velocity field, Vortex field.

1. Introduction

Ship resistance is a very important calculation and is obtained in the preliminary design stage. It is further used to predict the speed and powering which represent the fulfilment of the ship design requirements. Nowadays, the use of computers in preliminary ship design has greatly given some advantages, therefore using a computer application, a proper ship design could be gained into some alternative designs, and then it is also determined simultaneously based on the fulfilment of the requirements.

In recent years, some tools of CFD have been widely developed and involved in the application of ship design and ship research. Then, these CFD already have been used in the practical ship design for predicting flow around the hull, flow separations, wave contour, water resistance, wake field, hull-wave interaction, etc. Although CFD has been developed progressively in the past sixty years and widened available, it shall more be progressed in the future. Following, some researches that were conducted as showing the ability of CFD in order to investigate specifically ship resistance and flow around a ship are discussed systematically within the year 2010 to 2019 such as the simulation of ship resistance of EIIb push barge in shallow water using CFD software Ansys Fluent [1], the CFD validation for multi-fidelity CFD-based design optimization by combining a potential flow code (WARP) and a URANS code (CFDShip) [2], the incompressible turbulent free surface flow around the complex hull form of the DTMB 5415 model at two different speeds using the RANSE code CFX [3], and the proposed F-Spline procedure to carry out hydrodynamic optimizations of ship hull forms by using the commercial software SHIPFLOW and FS-Framework [4]. Those researchers discussed that were focused on the proposed CFD with its method for capable solving and optimizing the hull form and the fluid flow characteristics i.e., RANSE [1] combined with the homogeneous multiphase Eulerian–Eulerian fluid approach [3], URANS combined with the potential solver of BEM [2], and the proposed F-Spline for ship hull design and Rankine panel method [4]. Within this period, along with the development of the researchers related to ship CFD, the CFD progress for ship hydrodynamics which is reaching the milestone of providing first-generation simulation-based design tools were evaluated [5] and then the computational ship hydrodynamics has embraced the exascale computing era with multi-scale, multi-physics, and multi-phase ship flows on billion-point grids, resolving most scales of turbulence and bubbles or droplets.

Furthermore, although the achievements of the CFD in the ship hydrodynamic investigation have shown the high-fidelity solvers, the study conducted by using the CFD has remained to be extended into some applications such as the resistance and wave form of a fast ship model by using Reynolds Averaged Navier Stokes (RANS) equations and Star CCM+ solver combined Volume of Fluid (VOF) [6], the viscous wave-making resistance of six ships from the hull with different hull forms using the solver naoe-FOAM-SJTU [7], the FlowVision code as the CFD tool, integrating a new method of in-detail hull form design based on the wave-based optimization [8], the total resistance and simulate flow around Wigley and DTMB 5415 hull form using computational fluid dynamic (CFD) [9], and the steady ship resistance with a highly automated procedure using the Naval Hydro Pack [10]. Those studies are almost similar to the previous studies in proposing a method for capable solving and optimizing the hull form and the fluid flow characteristics.

The above discussion highlights the development of ship CFD that has robust results. Meanwhile, an application tool that could handle both object-oriented design and its calculation on ship hydrodynamics analysis is therefore required in order to obtain quickly a proper or optimum design in the preliminary design stage. However, CFD commercial software is very expensive and then for compensating the OpenSource CFD has been presented freely and is of great interest.

In the following, several studies have been conducted by using OpenSource CFD for predicting and investigating the ship resistance and flow around a ship such as the developed SNUFOAM [11], FVM using the OpenFOAM [12]. In additions, the other applications by using OpenFOAM were carried out to viscous wave-making resistance [7], various turbulent modeling [13], wave breaking around a high-speed surface combatant with artificial compression technique [14], manoeuvrability and resistance characteristics [15], two-phase flow solver HiFoam based on the OpenFOAM [16], hull resistance of a catamaran [17], and resistance in calm water and in waves for a ferry ship model [18]. In OpenFOAM, the interface capturing method is solved by using the VOF scheme, three-dimensional meshes of hexahedral are generated by using the snappyHexMesh, the structured grid is solved by using the Finite Volume Method (FVM), and the mathematical model is the RANS solver.

Concurrent with CFD development and enhancement by some researchers and ship design consultants, CFD workshop in ship hydrodynamics had been conducted by International Towing Tank Conference (ITTC) since 1980. ITTC [19, 20] provides a good practice guideline which can be applied to the most ship hydrodynamic application. Regardless, the validation of the numerical simulations is an essential way for the interpretation of the results, and the identification of those aspects of simulation is an effort that has to be improved continuously.

Based on those explanations previously, it must be noted that the progress of CFD for the investigation of ship hydrodynamics has been well conducted, nevertheless, these will be always developed and enhanced in future work to obtain a satisfied result. Furthermore, OpenFOAM, as open source, has been used rapidly by researchers and industries. On the other side, the open source, namely Autodesk CFD has a discretization method, Finite Element Method (FEM), and this seems different compared with OpenFOAM. Therefore, this present study has conducted the investigation of ship resistance, fluid velocity around a ship, and pressure distribution acting on a model's surface by using the Autodesk CFD. Moreover, the capability and accuracy of the Autodesk CFD for such investigation has been validated by comparing it with the experimental results. Therefore, the objective of this present study is to investigate a discrepancy of the ship resistance, pressure distribution as resulted from the Autodesk CFD and experimental investigation. Then the possibility of the use of Autodesk CFD for using in the preliminary ship design stage has been clarified based on the computer specifications, time cost, and validation results. Here, the free Autodesk CFD has not been used specifically yet in ship hydrodynamic investigation by researchers, and then in the present study, it has been applied and a technique of the box region was involved in the application. The free Autodesk CFD is for students and educator's version [21]. In addition, by using the piezoelectric device in the experimental performance, the pressure distribution acting on the ship surface as resulted by Autodesk CFD can be validated.

2. Computational Methods

2.1. Overview of Autodesk CFD

The finite element method (FEM) can be used in the fluid dynamic application with special techniques for a conservative solution. The FEM is much more stable compared with the other discretization methods. In Autodesk CFD [21, 22], the FEM is used to reduce the governing partial differential equations (PDES) to a set of algebraic equations. In this method, the dependent variables are represented by polynomial shape functions over a small area or volume (element). Then, the FEM is a particular numerical method for solving partial differential equations in two or three space variables and to predict the behaviour of each element. The result is a set of algebraic equations for the dependent variable at discrete points or nodes on every element. Correspondingly a real object into a large number of finite elements is analysed by using, a type of computerized analysis method, the finite element analysis (FEA). Autodesk CFD uses FEM primarily because of its flexibility in modeling any geometric shape such as linear for 3D tetrahedral elements (unstructured grids) wherein Galerkin's method of weighted residuals is generally used. Hence, the geometric flexibility inherent in finite elements has been maintained in Autodesk CFD.

2.2. Governing equations

The governing equations for fluid flow are the external incompressible flow of the Navier-Stokes or momentum equations [22]. The governing PDES for continuity equation can be written as:

$$\frac{\partial \rho}{\partial t}+\frac{\partial \rho u}{\partial x}+\frac{\partial \rho v}{\partial y}+\frac{\partial \rho w}{\partial z}=0 \tag{1}$$

where, ρ is the density, t is the time, u is the velocity component in x-direction, v is the velocity component in y-direction, and w is the velocity component in z-direction.

Then, X-Momentum, Y-Momentum, and Z-Momentum equations are derived from the continuity equation as follows. X-Momentum is given:

$$\begin{aligned}&\rho\frac{\partial u}{\partial t}+\rho u\frac{\partial u}{\partial x}+\rho v\frac{\partial u}{\partial y}+\rho w\frac{\partial u}{\partial z}\\&=\rho g_x-\frac{\partial u}{\partial t}+\frac{\partial u}{\partial x}\left[2\mu\frac{\partial u}{\partial x}\right]+\frac{\partial}{\partial y}\left[\mu\left(\frac{\partial u}{\partial y}+\frac{\partial v}{\partial x}\right)\right]\\&+\frac{\partial}{\partial z}\left[\mu\left(\frac{\partial u}{\partial z}+\frac{\partial w}{\partial x}\right)\right]+S_\omega+S_{DR}\end{aligned} \tag{2}$$

Y-Momentum equation is given:

$$\begin{aligned}&\rho\frac{\partial v}{\partial t}+\rho u\frac{\partial v}{\partial x}+\rho v\frac{\partial v}{\partial y}+\rho w\frac{\partial v}{\partial z}\\&=\rho g_y-\frac{\partial p}{\partial y}+\frac{\partial}{\partial x}\left[\mu\left(\frac{\partial u}{\partial y}+\frac{\partial v}{\partial x}\right)\right]+\frac{\partial}{\partial y}\left[2\mu\frac{\partial v}{\partial y}\right]\\&+\frac{\partial}{\partial z}\left[\mu\left(\frac{\partial v}{\partial z}+\frac{\partial w}{\partial y}\right)\right]+S_\omega+S_{DR}\end{aligned} \tag{3}$$

Z-Momentum equation is given:

$$\frac{\partial w}{\partial t}+\rho u\frac{\partial w}{\partial x}+\rho v\frac{\partial w}{\partial y}+\rho w\frac{\partial w}{\partial z}$$
$$=\rho g_z-\frac{\partial p}{\partial z}+\frac{\partial}{\partial x}\left[\mu\left(\frac{\partial u}{\partial z}+\frac{\partial w}{\partial x}\right)\right]+\frac{\partial}{\partial y}\left[\mu\left(\frac{\partial v}{\partial z}+\frac{\partial w}{\partial y}\right)\right]$$
$$+\frac{\partial}{\partial z}\left[2\mu\frac{\partial w}{\partial z}\right]+S_\omega+S_{DR} \quad (4)$$

where, g_x, g_y, g_z are the gravitational acceleration in *x*, *y*, *z* directions, μ is the viscosity, S_ω rotating flow, and S_{DR} is the distributed resistance term.

The two source terms in the momentum equations are $S\omega$ for rotating coordinates and S_{DR} distributed resistances, respectively. The distributed resistance term can be written in general as:

$$S_{DR}=-\left(K_i+\frac{f}{D_H}\right)\frac{\rho V_i^2}{2}-C\mu V_i \quad (5)$$

where, *V* is the velocity, *i* refers to the global coordinate direction (*u*, *v*, *w* momentum equation), *f* is the friction factor, *d* is the hydraulic diameter, *C* is the permeability. *K*-factor term can operate on a single momentum equation at a time because each direction has its own unique *K*-factor. The other two resistance types operate equally on each momentum equation.

The other source term is for rotating flow. This term can be written in general as:

$$S_\omega=-2\,\rho\omega_i\times V_i-\rho\omega_i\times\omega_i\times r_i \quad (6)$$

where, ω is the rotational speed and *r* is the distance from the axis of rotation.

For turbulence models, this study uses the wall function or *k-epsilon* (*k*-ε), *k* is the kinetic energy per unit mass and ε is the turbulent dissipation wherein it is suitable for the interactions of the external incompressible flow with complex geometry.

3. Computational Conditions

3.1. Ship data and model scale

The actual ship which was employed in this simulation is a general cargo type. There are two ship models in this simulation namely the model with a bulbous bow (BB) and without a bulbous bow (WBB). The principal particulars of the actual ship and the scaled models are provided in Table 1. The ship model scale is 1:40. The body plan of the actual ship is shown in Fig. 1.

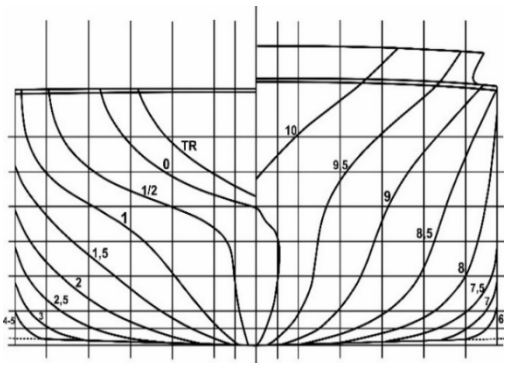

Fig. 1. Body plan of the actual ship.

3.2. Computational domain, boundary and mesh sizing conditions

For ship resistance test, the computational domain of a water tank is a rectangular block and a tetrahedral mesh as shown in Fig. 2, and then in this study, the size of the computational domain was considered the boundary conditions and the area of the flow directions to the free cross-section between the fluid region and solid region. Therefore, the size of the computational domain was decided sufficient large and matched the blockage correction of the width and depth between ship model and water tank for the ship resistance test wherein the size of the length is 4.57 *Lbp*, width is 2 *Lbp*, and depth 1 *Lbp* as defined in *x*, *y*, and *z*-directions, respectively. The fluid flow points *x*-direction, *y*-direction is the port-starboard of the flow direction, and the positive *z*-axis is upward. For the boundary conditions, the upstream inlet and far-field boundary were specified for velocity and turbulent properties and the reference pressure was applied downstream. A slip boundary was applied on the top, *Y*-min, and *Y*-max boundary. The boundary conditions in the computational domain are shown in Fig. 2. The material of the ship model was input as a solid (steel) phase and the water tank was liquid (seawater) phase.

Table 1. Principal particulars of ship and models.

Description	Actual Ship	WBB	BB
Length over all/*Loa* (m)	73.3	1.83	1.83
Length between perpendiculars/*Lbp* (m)	70.1	1.75	1.75
Breadth/*B* (m)	11.5	0.29	0.29
Draught/*D* (m)	7.0	0.18	0.18
Draft/*d* (m)	5.5	0.14	0.14
Wetted surface area (m^2)	1312.83	0.805	0.817

In this study, in order to obtain a high accuracy of the computational results, the box region was considered to build around the ship model for adding a fine mesh. The mesh size of the box region is suited with the solid mesh. By using the box region, the initial input and computational condition do not change during the simulation process.

On the other hand, the adequate number of meshes in order to ensure the accuracy of computation results also was examined by using the comparison result between the Autodesk CFD and experimental results at water velocity 0.894 m/s or Froude number (*Fr*) 0.213 for both model BB and WBB as shown in Tables 2 and 3, respectively. For model BB, case 3 which gives the small deviation was selected wherein the total mesh number of the fluid element is 8228836 and the solid element of the model BB is 1325809. Meanwhile, case 3 also was selected for the model WBB wherein the mesh number of the fluid and solid elements are 4277049 and 107820, respectively. The ship model meshing for both model BB and WBB is shown in Fig. 3.

In the Autodesk CFD, the convergence criteria by the ratio of the residual out and residual in are given 1.0E-08 for ensuring the stability and convergence of the analysis. In this study, the convergence of the pressure parameter was examined in the iteration of the simulation 300, and then the ratio of the residual in and residual out was obtained 4.22E-12 for BB simulation at Fr 0.213 and 1.70E-12 for WBB simulation at Fr 0.213. This means that the presence of computational simulation is stable.

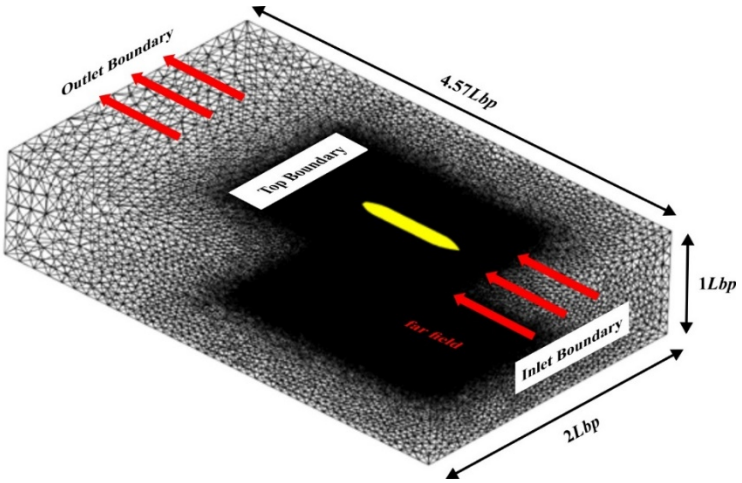

Fig. 2. Computational domain and boundary conditions.

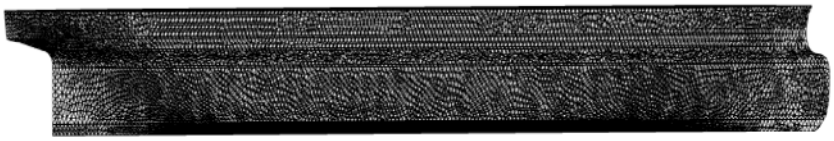

(a) Model BB meshing.

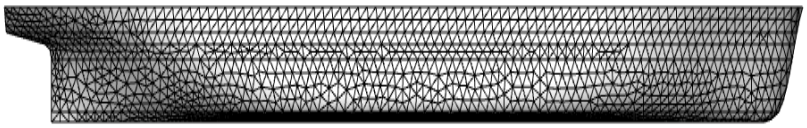

(b) Model WBB meshing.

Fig. 3. Ship model meshing.

Table 2. The mesh number of the BB simulation.

Case	Element	Mesh number	Fr	CFD	Exp.	Dev. (%)
1	Fluid element Solid element	824121 4725	0.213	2.618	2.393	8.59
2	Fluid element Solid element	821031 4748	0.213	2.594	2.393	7.75
3	Fluid element Solid element	8228836 1325809	0.213	2.516	2.393	4.89

Table 3. The mesh number of the WBB simulation.

Case	Element	Mesh number	Fr	CFD	Exp.	Dev. (%)
1	Fluid element Solid element	839354 4573	0.213	3.142	2.586	17.70
2	Fluid element Solid element	4222022 17876	0.213	2.769	2.586	6.61
3	Fluid element Solid element	4277049 107820	0.213	2.717	2.586	4.82

4. Results and Discussion

4.1. Computational results

The CFD simulations by using Autodesk CFD were successfully carried out by using some techniques as discussed in the section on the computational conditions and then the results are discussed accordingly. In this simulation, the fluid flow was in a steady-state and then turbulent flow was applied. The iteration number was 300 per model's velocity. In addition, the computational simulations were run in the increasing of the water velocity as assumed equal to the model's velocity from 0.081 m/s to 0.894 m/s or Froude number (Fr) 0.019 to 0.213. The maximum Fr set in the computational simulation was considered in the same maximum Fr of the actual ship.

4.1.1. Fluid velocity, pressure distribution, and vortex generation

The velocity field around WBB and BB has been captured within the box region on centre plane y = 1.0 *Lbp* as visualized in Fig. 4 wherein the initial input of the water velocity was set at 0.894 m/s or Fr 0.213.

The contour of the water velocity magnitude around BB and WBB is coded by the different colour (brightness). The flow velocity gradually decreases after hitting the bow part for both model BB and WBB. The boundary of the flow velocity around BB is different from WBB especially in the bottom and rear part wherein the velocity magnitude around BB is lower than WBB. This different magnitude impacts wake along with the model and pressure distribution along the model's body. Therefore, the effect of bow shape influences the flow velocity around the model.

The effect of the flow velocity around the model on pressure distribution acting on BB and WBB surface has been captured as shown in Fig. 5. The pressure distribution acts dominantly high on the bow region for both model BB and WBB at Fr 0.213. The range of the pressure coefficient shows the difference between model BB and WBB wherein the positive pressure coefficient of the model BB is higher than WBB whereas the negative pressure coefficient of the model WBB is lower than BB.

The peak pressure coefficient of the model BB is 1.073 and the lower pressure coefficient is -0.314. Meanwhile, for the model WBB, the peak pressure coefficient is 0.917 and the lower pressure coefficient is -0.416. The negative pressure coefficients act on the surface of the bow shoulder for both model BB and WBB. Also, the negative pressure impacts the bow shoulder region of both models, and this negative pressure can decrease the viscous pressure resistance.

On the other side, the inflow was driven by the forebody downstream and the flow momentum on the aft body generates a big vortex contour. The occurrence of the big contour shows the difference between model BB and WBB at Fr 0.213 as shown in Fig. 6. In the case of the BB, the wake occurs on the region of the bow shoulder to the mid-body as shown in Fig. 6(a) whereas it occurs behind the mid-body to the stern region as shown in Fig. 6(b).

The overall hydrodynamic parameters such as water velocity, pressure distribution, and vorticity that were obtained by using Autodesk CFD increase in the increasing Fr for both models WBB and BB.

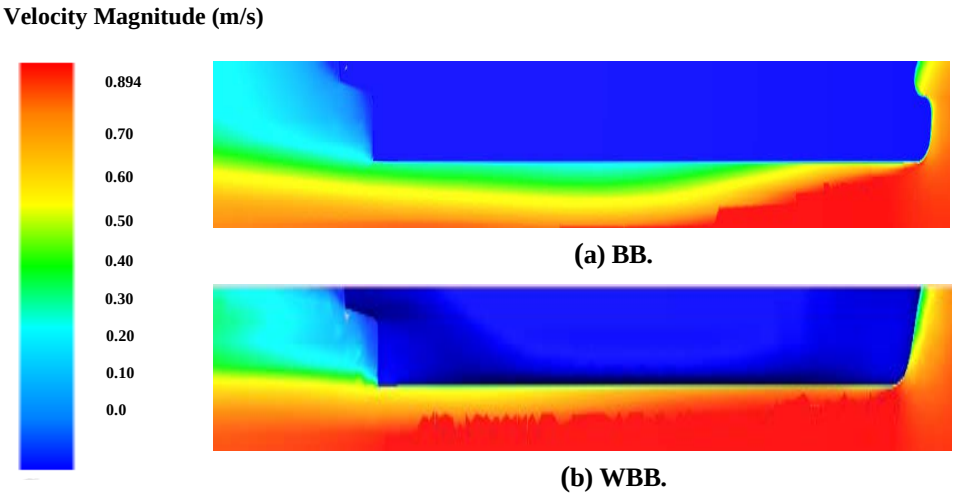

(a) BB.

(b) WBB.

Fig. 4. Velocity magnitude at Fr 0.213.

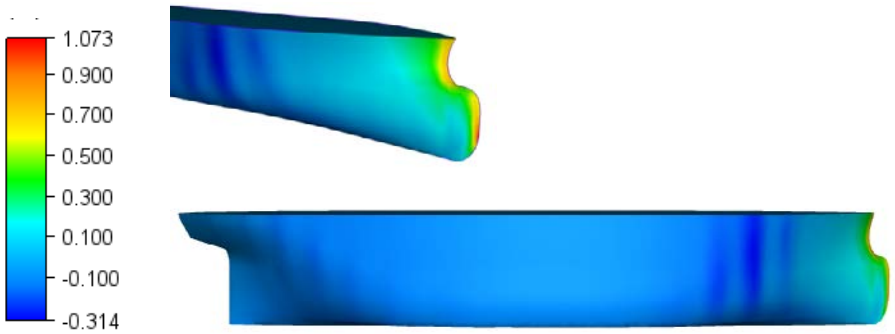

(a) BB.

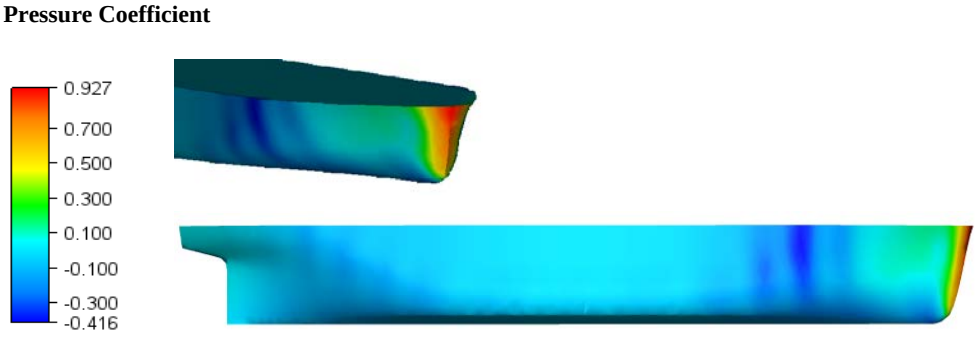

(b) WBB.

Fig. 5. Pressure distribution on hull surface at Fr 0.213.

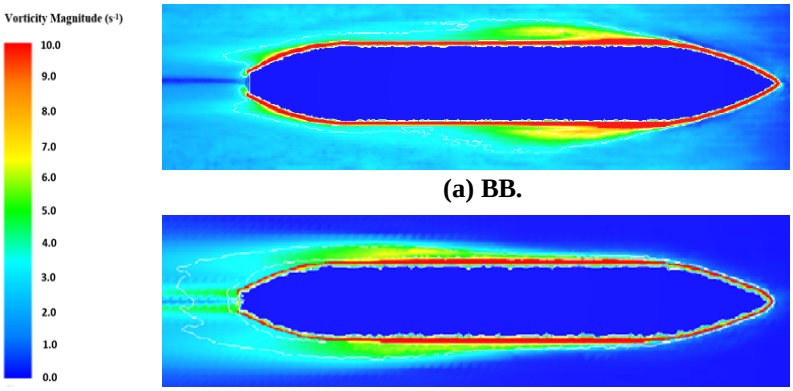

(a) BB.

(b) WBB.

Fig. 6. The vortex generation in flow field at Fr 0.213.

4.1.2. Ship resistance

Ship water resistance, as a total resistance (*Rt*), was predicted successfully and then the comparison of the water resistance between model BB and WBB was obtained as well. Figure 7 shows the tendency of water resistance coefficient in both model BB and WBB in the increasing of the Fr from 0.019 to 0.213. The coefficient of water resistance (*Ct*) is defined by $Rt/0.5\rho SV2$ wherein *S* is the wetted area and *V* is the model's velocity. This can be seen that the water resistance coefficient tends to decrease in the increasing of the Fr and the tendency of the water resistance coefficient for both model BB and WBB is similar. The coefficient of water resistance of the model WBB is higher than the model BB and the difference value of the water resistance coefficient is obtained 13.58%.

Although both models have the same geometric parameter of the length to beam ratio and a small difference only in the shape of the bow part, this Autodesk CFD application can distinguish the effect of the bulbous bow on the magnitude of viscous pressure drag as given the different value such the obtained coefficient of the water resistance *Ct*. The causes of this difference have been also depicted clearly by Figs. 4 to 6.

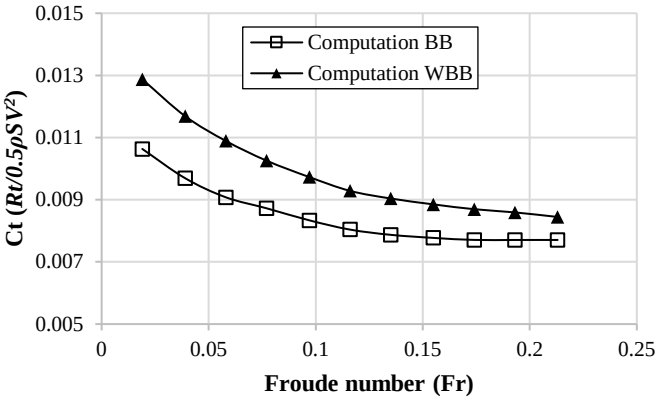

Fig. 7. The tendency of water resistance coefficient (*Ct*) in increasing *Fr*.

The physical time spent in this computational simulation was approximately 3.77 hours per case for model WBB and then 10.32 hours per case for model BB. The specifications of the laptop which was used in this study are Intel i7-8550U @ 1.99 GHz, RAM 16 GB, 64-bit operating system, and x64-based processor. Based on the time cost and laptop specifications, the investigation of ship resistance, pressure distribution, and vortex flow can be carried out by using the Autodesk CFD in the preliminary ship design stage. In the future study, a free surface flow along ship and other flow phenomena due to high speed will be conducted by using the transient analysis.

4.2. Experimental results

The experiments of both model BB and WBB on pressure distribution, wave profile, and water resistance were successfully conducted in Towing Tank, Ship Hydrodynamics Laboratory, Naval Architecture Department, Engineering Faculty, Hasanuddin University. The towing tank sizes are 60 m in length, 4 m in width, and 4 m in depth. Before using this new towing tank, the resistance of the same model is benchmarked conducted by the other towing tank. The speed of the towing carriage is a maximum of 4 m/sec. In the experimental works, the models had the same main dimensions as the computational models and several model's speeds were considered namely 0.244 m/s (Fr 0.058), 0.488 m/s (Fr 0.116), 0.732 m/s (Fr 0.174), and 0.894 m/s (Fr 0.213) as well those representative speeds, described the speed increase, could provide sufficient data to be used for validating the computational results. For the effects of a boundary due to the water flow around the model, the blockage effect was corrected by using Bmodel $<B$tank/10 to Btank/15 and $d$model $<h$tank/10 to $h$tank/20. The value of the blockage met with the correction range and was considered in this experimental work. Moreover, for the resistance experiment, the model was provided without the attachments of the piezoelectric device and its installations.

4.2.1. Pressure distribution

The pressure distributions that are acting on the model surface under water level were investigated experimentally with various Froude numbers. Figure 8 shows piezoelectric sensors which were attached and installed on both model surface BB and WBB. The piezoelectric sensor is connected to breadboard and Arduino mega and then these were installed to the computer as shown the block diagram in Fig. 9.

Figure 10 shows the examples of time history pressure distributions that are measured on *P1*, *P2*, *P3* and *P4* on the bow part of the model BB and WBB respectively at Fr 0.213. The time history of the pressure distributions was recorded in ten seconds. The average of the peak pressure acting on bow part BB are obtained *P1* 421.753 (N/m^2), *P2* 419.231 (N/m^2), *P3* 411.774 (N/m^2), and *P4* 378.710 (N/m^2) and then the average of the overall peak pressure magnitude *P1*, *P2*, *P3*, and *P4* are obtained 407.867 (N/m^2). For the peak pressure on the bow part, the average of the peak pressure is *P1* 506.584 (N/m^2), *P2* 470.754 (N/m^2), *P3* 210.933 (N/m^2), and *P4* 215.377 (N/m^2) and then the average of the overall peak pressure magnitude *P1*, *P2*, *P3*, and *P4* are obtained 350.912 (N/m^2). For the comparison of the average of the overall peak pressure acting on the bow part, the model BB is higher than model WBB and the difference is around 13.96%. Meanwhile, the average of the peak pressure on the stern part BB is obtained *P9* 46.706 (N/m^2), *P10* 113.073 (N/m^2),

P11 61.598 (N/m^2), and *P12* 61.598 (N/m^2) and then the average of the overall peak pressure is 70.744 (N/m^2).

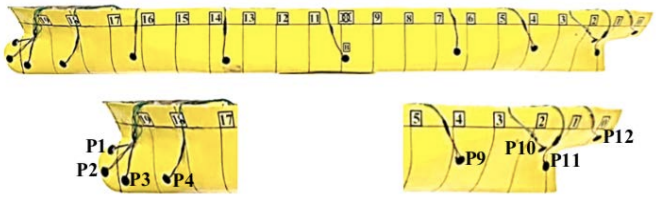

(a) BB.

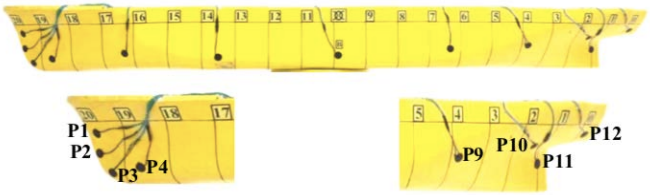

(b) WBB.

Fig. 8. The ship model with the attached piezoelectric.

Moreover, the average of the pressure distributions on the stern part WBB is *P9* 61.045 (N/m^2), *P10* 115.073 (N/m^2), *P11* 71.369 (N/m^2), and *P12* 72.428 (N/m^2) and then the average of the overall peak pressure is 79.978 (N/m^2). The average peak pressure of the model WBB is higher than model BB and it has a different value of approximately 11.55%. Although the peak pressure on bow part BB is sufficiently higher than WBB, in contrast, the peak pressure on stern part WBB is higher. As a result of higher peak pressure due to bulbous bow shape compared without the bulbous bow, this can be noted that the effect of the bulbous bow could reduce water pressure along the model's body and water intake (vortex field) after passing the bow part.

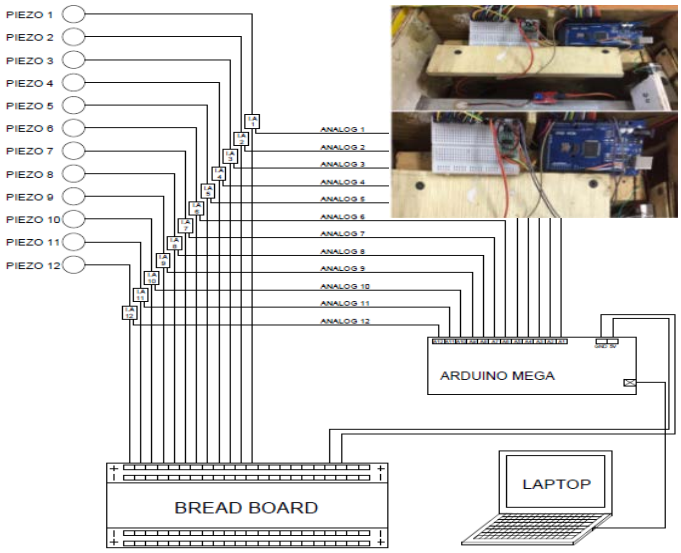

Fig. 9. Block diagram of piezoelectric sensor installation.

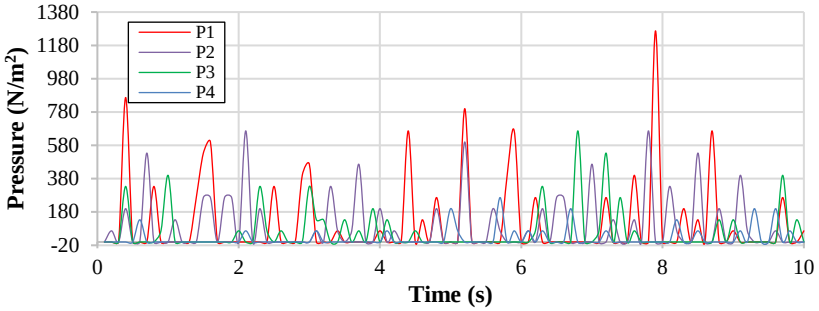

(a) BB.

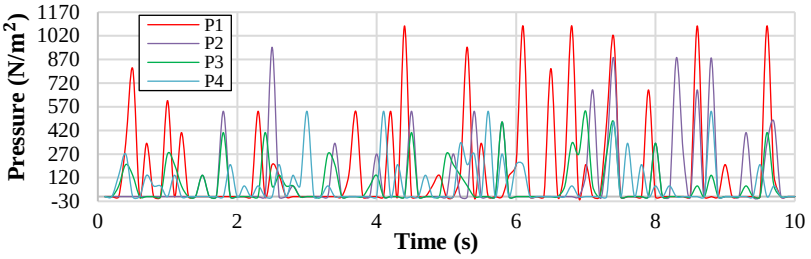

(b) WBB.

Fig. 10. Time history of pressure distribution on bow part at Fr 0.213.

Here, the pressure coefficient *Cp* is defined by $Pmax/0.5\rho V2$ wherein *Pmax* is peak pressure, ρ is water density, and *V* is water velocity. The peak pressure coefficient of the model BB is obtained 1.021 and for WBB it is obtained 0.878. For the comparison of the peak pressure coefficient on the bow part between the Autodesk CFD as shown in Fig. 5 and experimental result, the *Cp* of the model BB and WBB as resulted by the Autodesk CFD is higher than the experimental results and the difference is obtained around 4.88% and 5.23% respectively. Meanwhile, the *Cp* of the experiment result for BB and WBB on the stern part is 0.177 and 0.200, respectively. Those experimental *Cp* are in the range of the computational *Cp*. Therefore, the computational *Cp* of the model BB and WBB shows good agreement with the experimental result.

4.2.2. Ship resistance

Ship resistance of both model BB and WBB was carried out successfully by performing experiments in various increasing the Fr in 0.058, 0.116, 0.174, and 0.213. Figure 11 shows the model BB and WBB that were used in the experiment. Figure 12 shows the tendency of the water resistance coefficient *Ct* for the model BB and WBB between computational and experimental results. The tendency of the *Ct* between computational and experimental results shows similar as well the *Ct* of the computational results for both models are higher than the experimental results. For small Fr (≤ 0.075), the *Ct* between the experimental and computational result for model BB and WBB has a very small difference.

(a) BB.

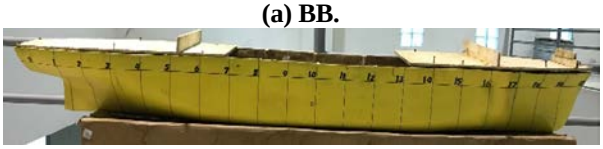

(b) WBB.

Fig. 11. Ship models for towing tank experiment.

The different value of the *Ct* between the computational and experimental result at Fr 0.058, 0.116, 0.174, and 0.213 for model BB is obtained 3.59% and then for model WBB, the different value is obtained 4.86%. Therefore, the overall computational water resistance coefficient *Ct* confirms good agreement with the experimental result.

Based on the time cost and laptop specifications for the computational simulation that have been discussed previously, the computational results of the ship resistance, pressure distribution has been validated with experimental results and then by the validation results, this adds an adequate reason for using widely the Autodesk CFD in the preliminary ship design stage.

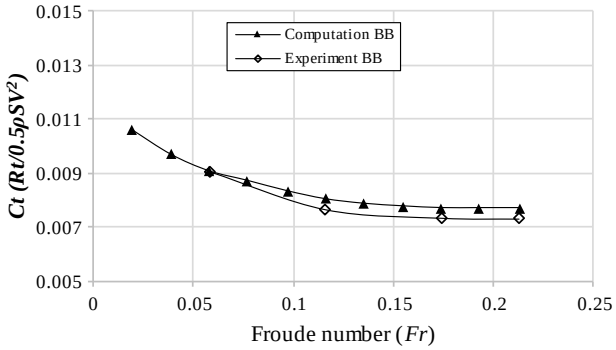

(a) BB.

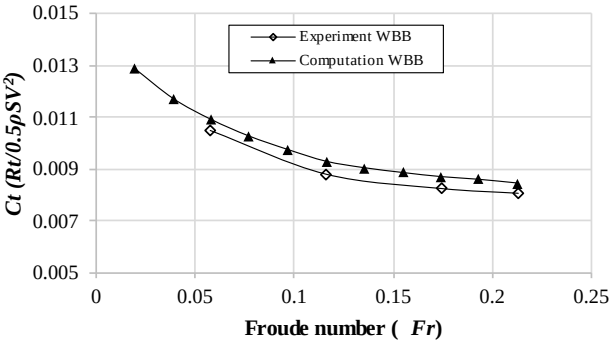

(b) WBB.

Fig. 12. The tendency of water resistance coefficient.

5. Conclusions

Herein the predictions of ship hydrodynamics by using the free application of Autodesk CFD were successfully conducted and then the dynamic parameters such as the velocity magnitude around the ship, pressure distribution on the ship hull, vortex field, and water resistance were obtained.

Correspondingly, the experimental works were carried out successfully as well to validate the obtained results of the free Autodesk CFD application. The comparisons of the coefficient peak pressure *Cp* on bow surface BB and WBB between the experimental and computational results are obtained the different magnitude around 4.88% and 5.23% respectively whereas the *Cp* of the computational result on stern part BB and WBB are in the same range magnitude with the experimental results. These *Cp* comparisons show good agreement.

Moreover, the computational results of the water resistance coefficient *Ct* in the increasing Fr have a similar tendency with the experimental results for both model BB and WBB. The different value of the *Ct* between the computational and experimental result at Fr 0.058, 0.116, 0.174, and 0.213 for model BB is obtained 3.59% and then for model WBB, the different value is obtained 4.86%. Therefore, the overall computational water resistance coefficient *Ct* confirms good agreement with the experimental result.

Based on the overall results above, the free Autodesk CFD application could be used practically in the preliminary ship design stage. In addition, a computer or laptop which is used for the computational simulation is recommended minimum specifications. In the future study, a free water surface along with the ship and other flow phenomena will be investigated by using the transient flow analysis provided by Autodesk CFD.

Acknowledgements

The authors would like to thank gratefully Ahmad Amsal Rasidi, Aji Prayoga, Rafika Arifin, Yance Mangalla, Muhammad Fadel Ramadhan and Abdul Wahid Hasim for their useful helps in conducting the computational simulation and experimental work.

Nomenclatures

C	Permeability, H/m
C_p	Pressure coefficient
Ct	Water resistance coefficient
f	Friction factor
Fr	Froude number
g_x	Gravitational acceleration in *x*-direction, m/s^2
g_y	Gravitational acceleration in *y*-direction, m/s^2
g_z	Gravitational acceleration in z-direction, m/s^2
k	Kinetic energy per unit mass, J/kg
K_i	*K*-factor term, m^{-1}
R_t	Total Resistance, N
r_i	Distance from the axis of rotation, m
S_{DR}	Distributed resistance term
S_ω	Rotating flow, s^{-1}

t	Time, s
u	Velocity of flow in x-direction, m/s
V_i	Velocity global coordinate direction, m/s
v	Velocity of flow in y-direction, m/s
w	Velocity of flow in z-direction, m/s

Greek Symbols

μ	Viscosity, Pa.s
ρ	Density, kg/m^3
Φ	Dissipation function
ω	Rotational speed, rad/s
ε	Turbulent dissipation, J/kg.s

Abbreviations

BB	Bulbous Bow
CFD	Computational Fluid Dynamics
FEM	Finite Element Method
FEA	Finite Element Analysis
FVM	Finite Volume Method
ITTC	International Towing Tank Conference
Lbp	Length between perpendicular
Loa	Length over all
OpenFOAM	Open-source Field Operation and Manipulation
PDES	Partial Differential Equations
RANS	Reynolds Averaged Navier Stokes
VOF	Volume of Fluid
WBB	Without Bulbous Bow

References

1. Benes, P.; and Kollarik, R. (2011). Preliminary computational fluid dynamics (CFD) simulation of EIIb push barge in shallow water. *Scientific Proceedings Faculty of Mechanical Engineering*, 19(1), 67-73.
2. Kandasamy, M.; Ooi, S.K.; Carrica, P.; Stern, F.; Campana, E.F.; Peri, D.; Osborne, P.; Cote, J.; Macdonald, N.; and Waal, N. (2011). CFD validation studies for a high-speed foil-assisted semi-planning catamaran. *Journal of Marine Science and Technology*, 16(2), 157-167.
3. Ahmed, Y.M. (2011). Numerical simulation for the free surface flow around a complex ship hull form at different Froude numbers. *Alexandria Engineering Journal*, 50(3), 229-235.
4. Han, S.; Lee, Y.-S.; and Choi, Y.B. (2012). Hydrodynamic hull form optimization using parametric models. *Journal of Marine Science and Technology*, 17, 1-17.
5. Stern, F.; Yang, J.; Wang, Z.; Sadat-Hosseini, H.; Mousaviraad, M.; Bhushan, S.; and Xing, T. (2013). Computational ship hydrodynamics: Nowadays and way forward. *International Shipbuilding Progress*, 60(1-4), 3-105.

6. Ozdemir, Y.H.; Barlas, B.; Yilmaz, T.; and Bayraktar, S. (2014). Numerical and experimental study of turbulent free surface flow for a fast ship model. *Brodogradnja/Shipbuilding*, 65(1), 39-54.
7. Zha, R.; Ye, H.; Shen, Z.; and Wan, D. (2014). Numerical study of viscous wave-making resistance of ship navigation in still water. *Journal of Marine Science and Application*, 13, 158-166.
8. Aksenov, A.A.; Pechenyuk, A.V.; and Vucinic, D. (2015). *Towards green marine technology and transport* (1st ed.). Chapter: Ship hull form design and optimization based on CFD. CRC Press, 215-223.
9. Ahmed, Y.M.; Yaakob, O.B.; Rashid, M.F.A.; and Elbatran, A.H. (2015). Determining ship resistance using computational fluid dynamics (CFD). *Journal of Transport System Engineering*, 2(1), 20-25.
10. Gatin, I.; Vukčević, V.; Škurić, V.; and Jasak, H. (2018). *Technology and science for the ships of the future*. Chapter: Fully automated ship resistance prediction using the naval hydro pack. IOS Press, 256-263.
11. Park, S.; Park, S.W.; Rhee, S.H.; Lee, S.B.; Choi J.-E.; and Kang, S.H. (2013). Investigation on the wall function implementation for the prediction of ship resistance. *International Journal of Naval Architecture and Ocean Engineering*, 5(1), 33-46.
12. Jasak, H.; Vukcevic, V.; and Christ, D. (2014). Rapid free surface simulation for steady-state hull resistance with FVM using OpenFOAM. *Proceedings of the 30th Symposium on Naval Hydrodynamics*. Tasmania, Australia, 1-7.
13. Axner, L.; Gong, J.; Chiarini, A.; and Mascellaro, L. (2014). SHAPE pilot monotricat SRL: Hull resistance simulations for an innovative hull using OpenFOAM. *Partnership for Advanced Computing in Europe*, 1-8.
14. Wang, J.; and Wan, D. (2017). Breaking wave simulations of high-speed surface combatant using OpenFOAM. *Proceedings of the 8th International Conference on Computational Methods*. Guangxi, China, 841-852.
15. Rahaman, M.M.; Islam, H.; Islam, M.T.; and Khondoker, M.R.H. (2017). Calm water resistance prediction of a bulk carrier using Reynolds averaged Navier-Stokes based solver. *AIP Conference Proceedings*, 1919(1), 1-6.
16. Kim, G.-H.; and Park, S. (2017). Development of a numerical tool for efficient and robust prediction of ship resistance. *International Journal of Naval Architecture and Ocean Engineering*, 9(5), 537-551.
17. Bustos, D.S.H.; and Alvarado, R.J.P. (2017). Numerical hull resistance calculation of a catamaran using OpenFOAM. *Ship Science and Technology*, 11(21), 29-39.
18. Islam, H.; and Soares, C.G. (2017). *Maritime transportation and harvesting of sea resources*. Chapter: Prediction of ship resistance in head waves using OpenFOAM. Taylor and Francis Group, 527-533.
19. ITTC. (2014). Practical guidelines for ship CFD applications (No. 7.5-03-0203). Retrieved August 21, 2019, from https://ittc.info/media/1357/75-03-02-03.pdf.
20. ITTC. (2014). Practical guidelines for ship resistance CFD (No. 7.5-03-0204). Retrieved August 21, 2019, from https://ittc.info/media/4198/75-03-02-04.pdf.

21. Autodesk CFD. (2017). Inventor: System requirements for Autodesk inventor 2017 products. Retrieved August 21, 2019, from https://www.autodesk.com/education/free-software/inventor-professional.
22. Autodesk CFD. (2017). Learning guide: General fluid flow and heat transfer equations. Retrieved August 21, 2019, from https://knowledge.autodesk.com/support/cfd/learn-explore/caas/CloudHelp/cloudhelp/2017/ENU/SimCFD-Learning/files/GUID-83A92AE5-0E9E-4E2D-B61F-64B3696E5F66-htm.html.